3-D Acquisition geometry analysis: incorporating information from multiples

Amarjeet Kumar, Gerrit Blacquière and Eric Verschuur, Delft University of Technology.*

SUMMARY

Recent advances in survey design have led to conventional common-midpoint-based analysis being replaced by the subsurface-based seismic acquisition analysis and design, with the emphasis on advance techniques of illumination analysis. Amongst them are wave-equation-based seismic illumination analyses such as the so-called focal beam method. The method's objective is to provide quantitative insight into the combined influence of acquisition geometry, overburden structure, and migration operators on image resolution and angle-dependent amplitude fidelity. So far, this method has only addressed illumination by primaries. However, multiples also contain information and may illuminate the target point from other angles than primaries, resulting in higher resolution and better illumination. In this paper, the focal beam analysis concept for multiple-reflected waves is introduced. The method demonstrates how the acquisition-related amplitude footprint can be corrected and improved using multiples.

INTRODUCTION

Since the last few decades, it has become clear that model-based seismic acquisition design is the key to further increase the value of the seismic method for the oil and gas industry. This is particularly true in the case of complex subsurfaces. Conventional survey design is based on the common-midpoint (CMP) analysis for a horizontally layered model and the quality of an acquisition geometry is generally judged by surface attributes such as CMP fold, bin-size, maximum offset, azimuth range (Cordsen et al., 2000; Vermeer, 2002; Galbraith, 2004). These subsurface-independent measures are just a first order approach as the influence of the subsurface is critical in seismic acquisition design. After all, the subsurface determines how the seismic source wavefields travel from the surface to the (potential) reservoir and how the reflected waves travel from the reservoir area back to the detectors at the surface. Therefore, information about the subsurface must be taken into account in any advanced method for seismic acquisition analysis and design.

At present, full-wavefield finite-difference modelling is widely used for wave propagation simulation but carrying out a full simulation of the seismic experiment and migrating the obtained synthetic seismic data is a computationally intensive way to obtain direct measures for image quality at the target (Jurick et al., 2003; Xie et al., 2006). There are, however, more efficient ways to obtain the same information without this sequence of modeling and migration.

A more efficient way is the so-called focal beam method, which was initially developed by Berkhout et al. (2001) and Volker et al. (2001), and further expanded by van Veldhuizen et al. (2008) and Wei et al. (2012). It makes use of the so-called common focus point (CFP) technology (Berkhout, 1997) in which a seismic response can be decomposed into grid-point responses, and the migration result can be simulated for a specific grid-point by double focusing (or bifocal imaging). This implementation enables accurate analysis for complex subsurfaces. It is a target-oriented method with a direct link to migration and reservoir characterization. Use of focal beams has the advantage that the influence of source geometry and detector geometry can be separately assessed. Thus, both target illumination by the source distribution and target sensing by the receiver distribution can be obtained. Combining this information yields knowledge about the resolution of migrated data and about the accuracy of angle-dependent amplitude information.

So far, only the primary signal was addressed in this method, leaving aside the multiples. Therefore, the migration response simulated for a specific grid point was similar to Kirchhoff migration. However, multiply scattered waves have the ability to reveal more information about the subsurface. These waves may illuminate structures that can not be easily illuminated by primaries and allow us to image portions of the subsurface not illuminated by singly scattered waves, resulting in a higher resolution and a better reservoir characterization. Therefore, multiples should not be treated as noise anymore. However, to make use of multiples in imaging, a better and more robust migration algorithm is needed. Over the last few years, the use of multiple reflections in seismic imaging has been discussed by many authors (Jiang et al., 2005; Whitmore et al., 2010; Berkhout and Verschuur, 2011; Lu et al., 2011; Davydenko and Verschuur, 2013).

We extended the focal beam theory, making use of all multiply scattered waves (surface-related as well as internal). In this paper, we discuss the theory, where we distinguish between illumination from above and illumination from below followed by the impact on the estimation of angle-dependent reflectivity.

GRID-POINT RESPONSE: INCLUDING MULTIPLES

We follow the matrix notation (Berkhout, 1982) in which a monochromatic component of the seismic wavefield with the j^{th} source at depth level z_n and k^{th} receiver at depth level z_m can be represented as a complex scalar $P_{kj}(z_m;z_n)$. Therefore, column-vector $\vec{P}_j(z_m;z_n)$ represents one shot record and matrix $\mathbf{P}(z_m;z_n)$ includes all shot records. Using this detail hiding operator notation, the monochromatic grid-point response for the full wavefield can be written as :

$$\delta_k\vec{P}_j^-(z_0;z_0) = \mathbf{D}(z_0)\mathbf{W}^-(z_0,z_m)\delta_k\mathbf{R}^{\cup}(z_m,z_m)\mathbf{G}^+(z_m,z_0)\vec{S}_j^+(z_0). \quad (1)$$

In this equation, j^{th} source $\vec{S}_j(z_0)$ at depth level z_0 propagates down by the full-wavefield operator $\mathbf{G}^+(z_m,z_0)$, towards depth level z_m, where it gets reflected by the k^{th} grid-point reflectivity matrix $\delta_k\mathbf{R}^{\cup}(z_m,z_m)$ and then propagates back to the surface level by one-way propagator $\mathbf{W}^-(z_0,z_m)$ and recorded at the detector matrix $\mathbf{D}(z_0)$ (Figure 1).

DOI http://dx.doi.org/10.1190/segam2014-1068.1

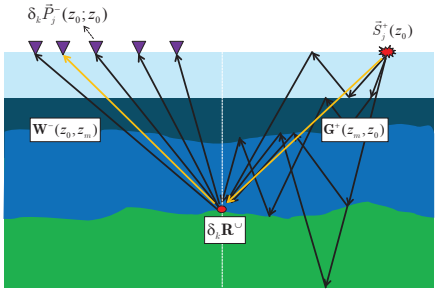

Figure 1: Full grid-point response. The yellow line shows the grid-point response for the primaries-only.

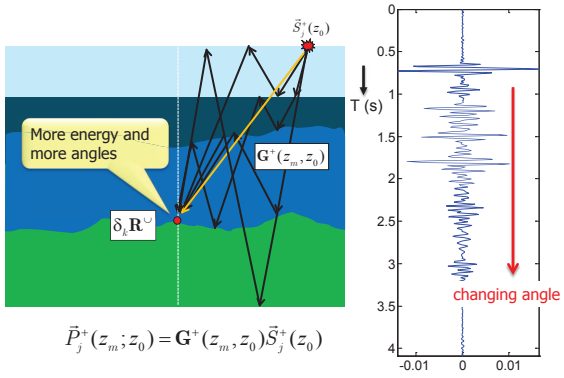

Figure 2: Illumination from above. Yellow line shows illumination by primaries-only. Note: multi-angle illumination is created by only one source.

For all J sources at the surface, the grid-point response matrix can be expressed as

$$\delta_k\mathbf{P}(z_0,z_0)=\left[\delta_k\vec{P}_1^-,....\delta_k\vec{P}_j^-,....\delta_k\vec{P}_J^-\right]. \qquad (2)$$

ILLUMINATION FROM ABOVE

Method

The term on the right hand side of the grid-point reflectivity matrix $\delta_k\mathbf{R}^\cup(z_m,z_m)$ of equation (1) represents the source side of the experiments, incidenting at the grid-point from above, and therefore known as illuminating wavefield from above (Figure 2). It can be expressed as:

$$\vec{P}_j^+(z_m;z_0)=\mathbf{G}^+(z_m,z_0)\vec{S}_j^+(z_0). \qquad (3)$$

Similarly, the left hand side of equation (1) corresponds to the detector side known as sensing wavefield. In the above formulation of grid-point response, all the complex wave paths by the multiples are kept on the source side, leading to a complex illuminating wavefield and a simple sensing wavefield. By doing so, detector side focusing would be a relatively easier step than source side focusing in seismic imaging.

Figure 2 explains why the multiples provide additional angles of illumination leading to multi-angle illumination from one shot record. Note that much more energy (sum of the squared amplitudes) is arriving at the grid-point than in the case of the primaries-only (shown in yellow). Moreover, this energy is arriving from different angles.

Previously in the focal beam theory, reflection properties of the k^{th} grid-point used to be computed by the double focusing of the grid-point response $\delta_k\mathbf{P}(z_0;z_0)$ as following:

$$\left\langle\vec{R}_k^\dagger(z_m,z_m)\right\rangle=\vec{F}_k^\dagger(z_m,z_0)\delta_k\mathbf{P}(z_0;z_0)\mathbf{F}(z_0,z_m). \qquad (4)$$

where inverse wave propagator $\mathbf{F}(z_0,z_m)$ is usually approximated by $\mathbf{W}^H(z_0,z_m)$. The symbol '†' indicates a row vector. This direct way of estimating reflectivity may be accurate enough in the case of a primaries-only wavefield because the inverse of a one-way propagator can be accurately approximated by its complex conjugate. However in the case of a full wavefield, one-way propagator $\mathbf{W}$ is replaced by two-way propagator $\mathbf{G}$ and the inverse of $\mathbf{G}$ can not be accurately approximated by its complex conjugate. Therefore, it must be computed by some minimization scheme. This will be discussed next.

At first, the modeled grid-point response (equation 2) is focused at grid-point k at z_m from the detector side. This yields the focus-point response, so-called CFP gather (Thorbecke, 1997). Here, the traces of the CFP gather are located at the position of the involved sources. Next, the focusing at the source side to find $\vec{R}_k^\dagger(z_m,z_m)$ is done by minimizing the following objective function using a conjugate gradient method:

$$J=\left\|\vec{F}_k^\dagger(z_m,z_0)\delta_k\mathbf{P}(z_0;z_0)-\vec{R}_k^\dagger(z_m,z_m)\mathbf{P}^+(z_m;z_0)\right\|_2^2. \qquad (5)$$

For the purpose of survey design analysis, the aim will not be to find the angle-dependent reflectivity but to find the angle-dependent footprint introduced by the acquisition geometry. Therefore, angle-dependent grid-point responses in the modeling can be replaced by angle-independent grid-point responses, i.e., by unit point diffractors. In that case, the results obtained by minimizing equation (5) provide the source beam, if the detectors are focused perfectly and vice versa.

The source and detector beams can be combined (multiplied) to a full migration result; an image of the target point (the resolution function). A plane wave decomposition of these beams by means of a Radon transform will provide the target illumination and the target sensing, respectively. By multiplication of the Radon transformed beams, the amplitude versus ray-parameter (AVP) function is obtained. This function shows the angle-dependent amplitude footprints at the target point that are caused by the acquisition geometry.

Example

To illustrate the advantage of using multiples, a 3-D model is considered. The velocity and reflectivity model are shown in Figure 3. At about 400 m depth there is an ellipsoidal high velocity area with a velocity of 3500 m/s. The reflectivity model has free-surface reflectivity as well.

The 3-D acquisition geometry comprises of a densely sampled detector spread and 8 source lines of 2000 m aperture with a sampling interval of 25 m along the x-direction as shown in

DOI http://dx.doi.org/10.1190/segam2014-1068.1

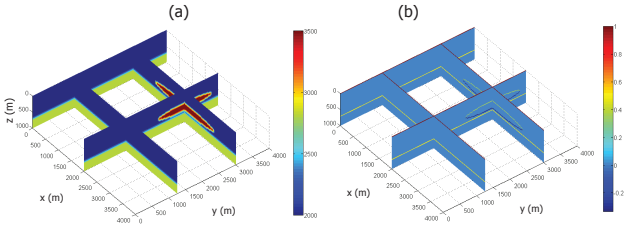

Figure 3: a) The velocity model; b) The reflectivity model.

Figure 4. A target point located at (x,y,z = 2000,2000,700) m in the subsurface has been chosen for the analysis. The source geometry has been taken such that it can illuminate the considered target point from large angles in the case of using the primaries-only incident wavefield. We will show that the smaller angles can be obtained by using multiples.

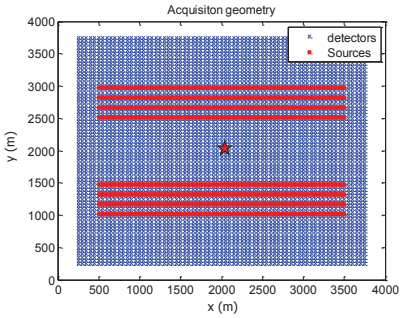

Figure 4: 3-D acquisition geometry. The target point is indicated by the red star.

The focal beam analysis was carried out for the above example using equation (5) and the results are shown in Figure 5. Figure 5a, b and c show the detector beam, the source beam and the AVP function for the primaries-only wavefield, respectively in the ray-parameter domain. Note that the detector beam shows that all angles are sensed as expected from the densely sampled detector spread. On the other hand, the source beam indeed shows only large illumination angles, consequently the AVP function also shows large reflection angles only. Similarly Figure 5d, e and f show the detector beam, the source beam and the AVP function for the full wavefield from above, respectively. Note the extension of illumination and reflection angles in the source beam and the AVP functions towards smaller angles.

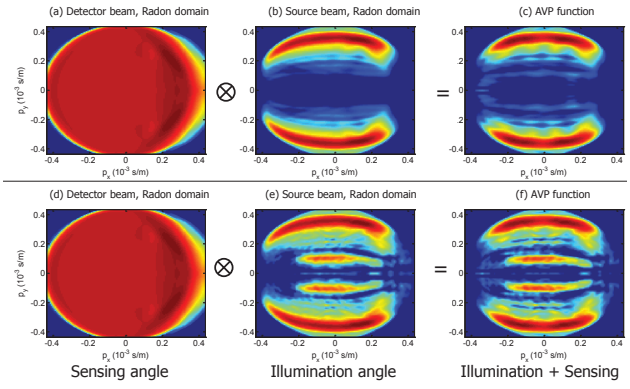

Figure 5: The detector beam, the source beam and the AVP function in the Radon domain for the primaries-only (first row) and the full-wavefield from above (second row).

ILLUMINATION FROM BELOW

Interestingly, by including all multiples, the target level will not only be illuminated by the incident source wavefield from above but also from below by the reflected wavefield from the deeper layers, as shown in Figure 6. In this case, we rely completely on multiples.

To compute the target illumination from below, the incident wavfield $\mathbf{P}^{+}(z_m;z_0)$ in equation (5) should be replaced by the incident wavefield from below $\mathbf{P}^{-}(z_m;z_0)$. In a very similar way, Figure 7a, b and c show the result of beams and AVP function in the case of illumination from below. It can be noticed in Figure 7b that illumination angles from below are complementary to those from above. The total illumination and reflection angles - from above and from below - are shown in Figure 7e and f, respectively.

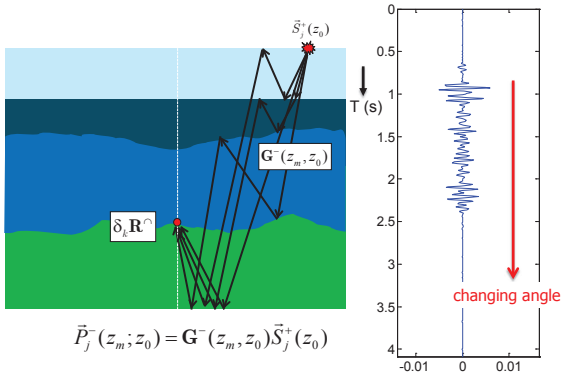

Figure 6: Illumination from below. Note: there is no direct wavefield in illumination from below.

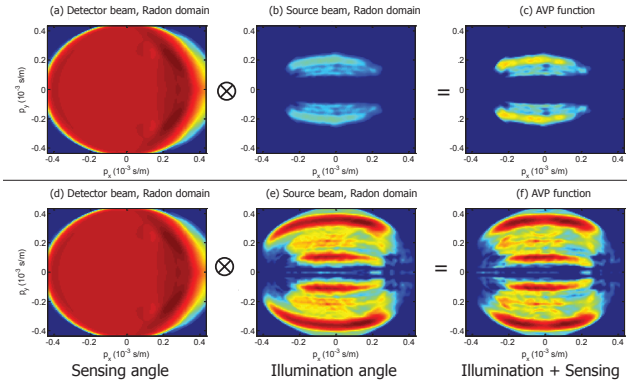

Figure 7: same as Figure 5 but for the illuminating wavefield from below (first row) and the total wavefield (second row).

DOI http://dx.doi.org/10.1190/segam2014-1068.1

IMPACT ON ANGLE-DEPENDENT REFLECTIVITY

The AVP function as presented in the previous section can be used to correct for an angle-dependent amplitude imprint caused by acquisition, overburden and processing. The reflection amplitude ($\widetilde{\mathbf{R}}_k$) found in the seismic data is always obscured by the acquisition AVP imprint ($\widetilde{\mathbf{A}}$), which leads to the measured reflectivity $\widetilde{\mathbf{A}}\widetilde{\mathbf{R}}_k$. The tilde symbol indicates the ray-parameter domain. The focal beam analysis provides a modeled AVP imprint, which represents an estimate of the true acquisition AVP imprint ($\widetilde{\mathbf{A}}$). Thus, the AVP imprint correction can be applied to the seismic data based on the estimated AVP imprint as follows:

$$\left\langle \widetilde{\mathbf{R}}_k \right\rangle = \left\langle \widetilde{\mathbf{A}} \right\rangle^{-1} \widetilde{\mathbf{A}}\widetilde{\mathbf{R}}_k. \qquad (6)$$

We computed the true angle-dependent reflectivity for the considered target point in the above example using the known contrast parameter. To estimate this angle-dependent reflectivity curve, the target point should be illuminated from all angles. Figure 8a and b show the true reflectivity curve ($\widetilde{\mathbf{R}}_k$) with blue lines, the measured reflectivity $\widetilde{\mathbf{A}}\widetilde{\mathbf{R}}_k$ with dotted black lines and the AVP imprint corrected reflectivity ($\left\langle \widetilde{\mathbf{A}} \right\rangle^{-1} \widetilde{\mathbf{A}}\widetilde{\mathbf{R}}_k$) with dotted red lines in the case of using primaries-only wavefield and the full wavefield, respectively. It can be seen that more angle-dependent information can be retrieved with the help of multiples.

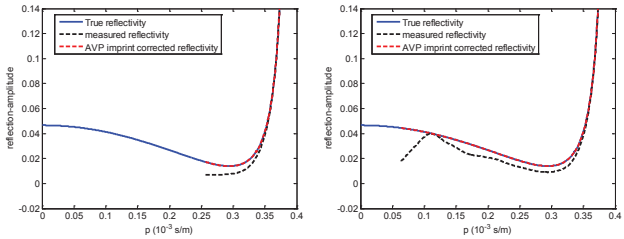

Figure 8: a) True reflectivity, measured reflectivity and the AVP imprint corrected reflectivity for the primaries-only wavefield; b) same for the full-wavefield.

It is important to notice here that these results have been obtained for the noise free case. Obviously in the presence of noise, the full-wavefield result is expected to give a more reliable, stable estimate of the reflectivity than the primaries-only wavefield result.

ZIGGY MODEL EXAMPLE

The Ziggy model is a Gulf of Mexico salt model developed by SMAART, a joint venture of BP, BHP Billiton, and Cheveron Texaco. The total dimensions of the model are 37 km (x) by 40 km (y) by 10 km (z). A small part of this model with dimensions of 5 km (x) by 5km (y) by 3 km (z) was extracted for the illumination analysis, which is shown in Figure 9a. The source geometry consists of 19 source lines in the *y*-direction, with a sampling interval of 250 m along the *y*-direction and

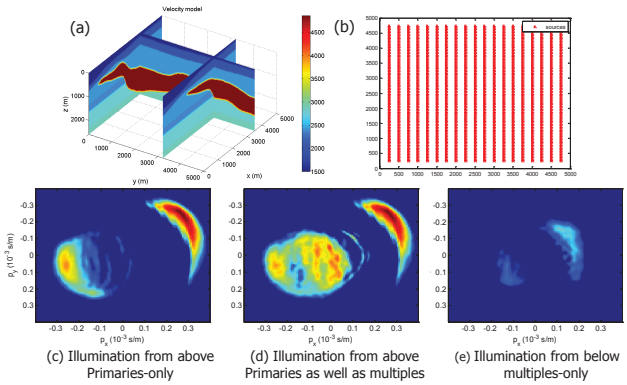

Figure 9: a) Part of the Ziggy model; (b) Source geometry (c) illumination angles for the primaries-only wavefield. (d) illumination angles for the full wavefield incidenting from above. (e) illumination angles for the multiples wavefield incidenting from below.

50 m along the *x*-direction, respectively, see Figure 9b. A target point located at (*x*,*y*,*z* = 2500,2500,2600) m in the subsurface has been chosen for the illumination analysis and the frequency range is 5 Hz to 30 Hz. It is important to mention here that the reflectivity model is required to analyze illumination by the internal multiples.

Again, equation (5) was solved to find the target illumination for the considered target point. Figure 9c shows the angles by which the considered target point is illuminated from the available sources at the surface in the case of using the primaries-only wavefield. Note that this very regular source distribution provides limited illumination only at the target point in the presence of the salt. In this type of scenarios, the multiply scattered wavefield help tremendously to extend the illumination where the singly reflected wavefield fails. Figure 9d and e show the extension in illumination angles (especially for smaller angles) in the case of using the full-wavefield incidenting from above and from below, respectively.

CONCLUDING REMARKS

The so-called focal beam method was expanded further to include analysis of having advantage from multiples. As a result of the complex illuminating wavefields involved, the source beam needs to be computed by a minimization scheme.

Illumination from above as well as from below by multiply reflected wavefields reveals information at angles that may not be present in primary illumination. In addition to that, the benefits from multiples increase with increasing complexity of the medium. This extended analysis via focal beams can be used for effective survey design, assuming that multiples will be used in imaging and reservoir characterization on a routine basis.

ACKNOWLEDGMENTS

The authors thank the sponsoring companies of the Delphi consortium and NAM for their financial support.

DOI http://dx.doi.org/10.1190/segam2014-1068.1

http://dx.doi.org/10.1190/segam2014-1068.1

EDITED REFERENCES

Note: This reference list is a copy-edited version of the reference list submitted by the author. Reference lists for the 2014 SEG Technical Program Expanded Abstracts have been copy edited so that references provided with the online metadata for each paper will achieve a high degree of linking to cited sources that appear on the Web.

REFERENCES

Berkhout, A. J., 1982, Seismic migration, imaging of acoustic energy by wavefield extrapolation, A: Theoretical aspects: Elsevier.

Berkhout, A. J., 1997, Pushing the limits of seismic imaging, part I: Prestack migration in terms of double dynamic focusing: Geophysics, **62**, 937–953, http://dx.doi.org/10.1190/1.1444201.

Berkhout, A. J., L. Ongkiehong, A. W. F. Volker, and G. Blacqui`ere, 2001, Comprehensive assessment of seismic acquisition geometries by focal beams — Part I: Theoretical considerations: Geophysics, **66**, 911–917, http://dx.doi.org/10.1190/1.1444981.

Berkhout, A. J., and D. J. Verschuur, 2011, Full wavefield migration, utilizing surface and internal multiple scattering: 81st Annual International Meeting, SEG, Expanded Abstracts, 3212–3216.

Cordsen, A., M. Galbraith, and J. Peirce, 2000, Planning land 3D seismic surveys: SEG.

Davydenko, M., and D. J. Verschuur, 2013, Full wavefield migration, using internal multiples for undershooting: Presented at the 83rd Annual International Meeting, SEG.

Galbraith, M., 2004, A new methodology for 3D survey design: The Leading Edge, **23**, 1017–1023, http://dx.doi.org/10.1190/1.1813363.

Jiang, Z., J. Yu, G. T. Schuster, and B. E. Hornby, 2005, Migration of multiples: The Leading Edge, **24**, 315–318, http://dx.doi.org/10.1190/1.1895318.

Jurick, D., J. Codd, F. Hoxha, J. Naumenko, and D. Kessler, 2003, Gulf of Suez acquisition design using 2D and 3D full wave equation simulation: 73rd Annual International Meeting, SEG, Expanded Abstracts, 2136–2139.

Lu, S., N. Whitmore, A. Valenciano, and N. Chemingui, 2011, Imaging of primaries and multiples with 3d seam synthetic: 81st Annual International Meeting, SEG, Expanded Abstracts, 3217–3221.

Thorbecke, J. W., 1997, Common focus point technology: Ph.D. thesis, Delft University of Technology.

van Veldhuizen, E. J., G. Blacquière, and A. J. Berkhout, 2008, Acquisition geometry analysis in complex 3D media: Geophysics, **73**, no. 5, Q43–Q58, http://dx.doi.org/10.1190/1.2972029.

Vermeer, G. J. O., 2002, 3D seismic survey design: SEG.

Volker, A. W. F., G. Blacquière, A. J. Berkhout, and L. Ongkiehong, 2001, Comprehensive assessment of seismic acquisition geometries by focal beams — Part II: Practical aspects and examples: Geophysics, **66**, 918–931, http://dx.doi.org/10.1190/1.1444982.

Wei, W., L. Fu, and G. Blacquière, 2012, Fast multifrequency focal beam analysis for 3D seismic acquisition geometry: Geophysics, **77**, no. 2, P11–P21, http://dx.doi.org/10.1190/geo2010-0327.1.

Whitmore, N., A. Valenciano, and W. Sollner, 2010, Imaging of primaries and multiples using a dual-sensor towed streamer: 80th Annual International Meeting, SEG, Expanded Abstracts, 3187–3192.

Xie, X., S. Jin, and R. Wu, 2006, Wave-equation-based seismic illumination analysis: Geophysics, **71**, no. 5, S169–S177, http://dx.doi.org/10.1190/1.2227619.

DOI http://dx.doi.org/10.1190/segam2014-1068.1